Acta Mech 227, 601–615 (2016)
DOI 10.1007/s00707-015-1480-6

ORIGINAL PAPER

S. Montero · R. Bustamante · A. Ortiz-Bernardin

A finite element analysis of some boundary value problems for a new type of constitutive relation for elastic bodies

Received: 22 July 2015 / Revised: 31 August 2015 / Published online: 22 October 2015

Abstract Recently, there has been interest in the study of a new class of constitutive relation, wherein the linearized strain tensor is assumed to be a function of the stresses. In this communication, some boundary value problems are solved using the finite element method and the solid material being described by such a constitutive relation, where the stresses can be arbitrarily 'large', but strains remain small. Three problems are analyzed, namely the traction of a plate with hyperbolic boundaries, a plate with a point load, and the traction of a plate with an elliptic hole. The results for the stresses and strains are compared with the predictions that are obtained by using the constitutive equation of the classical linearized theory of elasticity.

1 Introduction

Some new types of constitutive relation have been proposed recently for the modelling of elastic bodies [2,5,6,25–31]. One such class corresponds to an implicit relation of the form $\mathfrak{F}(\mathbf{T}, \mathbf{B}) = \mathbf{0}$, where $\mathbf{T}$ is the Cauchy stress tensor and $\mathbf{B}$ is the left Cauchy–Green strain tensor. As presented, for example, in Section 2.2 of [25], if one considers the case $|\nabla \mathbf{u}| \sim O(\delta)$, $\delta \ll 1$, the approximation $\mathbf{B} \approx 2\boldsymbol{\varepsilon} + \mathbf{I}$ is obtained and from $\mathfrak{F}(\mathbf{T}, \mathbf{B}) = \mathbf{0}$ we have the relation $\boldsymbol{\varepsilon} = \mathfrak{f}(\mathbf{T})$. The latter class of constitutive equation is very interesting on its own and has been studied in different works [3–10,13,21,24,25,31]. About some possible applications of $\boldsymbol{\varepsilon} = \mathfrak{f}(\mathbf{T})$, we mention, for example, the modelling of some metal alloys [32,34], rock[1] [17], and the analysis of cracks in brittle bodies [3,4,13,21]. For brittle bodies, expressions for $\mathfrak{f}$ such that $\boldsymbol{\varepsilon}$ remains small independently of how big $|\mathbf{T}|$ is, can be of great interest in the study of stress concentration problems, where from the experimental point of view 'large' stresses,[2] elastic behaviour, and small strains are expected (see [31] for a thorough discussion on the potential use of $\boldsymbol{\varepsilon} = \mathfrak{f}(\mathbf{T})$).

Considering the number of possible applications for the new class of constitutive equation $\boldsymbol{\varepsilon} = \mathfrak{f}(\mathbf{T})$, it is important to solve different boundary value problems using such relations. This has been done, for example, in [7–9,19,24,25] using exact and numerical methods. In the present work, the finite element method is used in order to study three problems where strain-limiting behaviour and concentration of stresses are present. This paper is organized as follows: in Sect. 2, a summary of the important equations is presented giving some details about the new class of above-mentioned constitutive relations for elastic bodies. Section 3 provides results for a thin plane plate with hyperbolic boundaries (see Sect. 3.1), for the problem of a semi-infinite medium (plane stress case) under the influence of a concentrated load (see Sect. 3.2), and finally, Sect. 3.3 provides results for

[1] If in a first approximation we assume that rock can be modelled as an elastic material.

[2] In order to be able to speak about large or small stresses, we need to compare $|\mathbf{T}|$ with some characteristic values for the stresses, which can be denoted by σ_0.

S. Montero · R. Bustamante (✉) · A. Ortiz-Bernardin
Departamento de Ingeniería Mecánica, Universidad de Chile, Beauchef 851, Santiago Centro, Santiago, Chile
E-mail: rogbusta@ing.uchile.cl
Fax: +56-2-6896057

the case of a plate with an elliptic hole under traction, where one of the semi-axes is very small in comparison with the other, thereby complementing the results for the same problem that were presented in [25].

This work is based on the results that are presented in the Master's thesis by Montero [22].

2 Basic equations

2.1 Kinematics and equation of equilibrium

Let X denote a point of a body $\mathscr{B}$. The reference configuration is denoted by $\kappa_r(\mathscr{B})$, and the position of each particle in that configuration is denoted by $\mathbf{X}$. The position of the same particle at time t in the current deformed configuration is denoted by $\mathbf{x}$, where the current configuration is $\kappa_t(\mathscr{B})$. It is assumed there exists a one-to-one mapping $\boldsymbol{\chi}$ such that $\mathbf{x} = \boldsymbol{\chi}(\mathbf{X}, t)$. The deformation gradient $\mathbf{F}$, the left Cauchy–Green deformation tensor $\mathbf{B}$, the displacement field $\mathbf{u}$, and the linearized strain tensor $\boldsymbol{\varepsilon}$ are defined, respectively, as

$$\mathbf{F} = \frac{\partial \mathbf{x}}{\partial \mathbf{X}}, \quad \mathbf{B} = \mathbf{F}\mathbf{F}^{\mathrm{T}}, \quad \mathbf{u} = \mathbf{x} - \mathbf{X}, \quad \boldsymbol{\varepsilon} = \frac{1}{2}\left(\nabla_X \mathbf{u} + \nabla_X \mathbf{u}^{\mathrm{T}}\right), \tag{1}$$

where it is assumed that $J = \det \mathbf{F} > 0$ and where ∇_X is the gradient operator with respect to the reference configuration.[3] More details about the kinematics of deformable bodies can be found, for example, in [11,36].

In this paper, time effects are not considered. The Cauchy stress tensor is denoted by $\mathbf{T}$ and must satisfy the equilibrium equation (quasi-static deformations)

$$\operatorname{div} \mathbf{T} + \rho \mathbf{b} = \mathbf{0}, \tag{2}$$

where ρ is the density of the body and $\mathbf{b}$ corresponds to the body forces in the current configuration.

2.2 Constitutive relations

Rajagopal and co-workers [26,28–30] have proposed some new classes of constitutive relations for elastic bodies, which cannot be classified as neither Cauchy nor Green elastic bodies. Let us consider in particular the implicit relation

$$\mathfrak{F}(\mathbf{T}, \mathbf{B}) = \mathbf{0}, \tag{3}$$

which in case that $\mathfrak{F}$ is an isotropic relation (see [33]) becomes

$$\begin{aligned} &\alpha_0 \mathbf{I} + \alpha_1 \mathbf{B} + \alpha_2 \mathbf{B}^2 + \alpha_3 \mathbf{T} + \alpha_4 \mathbf{T}^2 + \alpha_5(\mathbf{B}\mathbf{T} + \mathbf{T}\mathbf{B}) + \alpha_6(\mathbf{B}\mathbf{T}^2 + \mathbf{T}^2\mathbf{B}) + \alpha_7(\mathbf{B}^2\mathbf{T} + \mathbf{T}\mathbf{B}^2) \\ &\quad + \alpha_8(\mathbf{B}^2\mathbf{T}^2 + \mathbf{T}^2\mathbf{B}^2) = \mathbf{0}, \end{aligned} \tag{4}$$

where α_j, $j = 0, 1, 2, \ldots, 8$ are scalar functions that depend on the invariants tr $\mathbf{B}$, $\frac{1}{2}$tr $\mathbf{B}^2$, $\frac{1}{3}$tr $\mathbf{B}^3$, tr $\mathbf{T}$, $\frac{1}{2}$tr $\mathbf{T}^2$, $\frac{1}{3}$tr $\mathbf{T}^3$, tr $(\mathbf{B}\mathbf{T})$, tr $(\mathbf{B}^2\mathbf{T})$, tr $(\mathbf{T}^2\mathbf{B})$, tr $(\mathbf{T}^2\mathbf{B}^2)$ and $\mathbf{I}$ is the identity tensor. In [25] (see Sect. 2.2 therein), it has been proved that when $|\nabla \mathbf{u}| \sim O(\delta)$, $\delta \ll 1$, and using the approximation $\mathbf{B} \approx 2\boldsymbol{\varepsilon} + \mathbf{I}$, Eq. (4) can be used to obtain

$$\boldsymbol{\varepsilon} = \mathfrak{f}(\mathbf{T}) = \gamma_0 \mathbf{I} + \gamma_1 \mathbf{T} + \gamma_2 \mathbf{T}^2, \tag{5}$$

where γ_0, γ_1, and γ_2 are scalar functions that depend on the invariants (see, for example, [25])

$$I_1 = \operatorname{tr} \mathbf{T}, \quad I_2 = \frac{1}{2}\operatorname{tr} \mathbf{T}^2, \quad I_3 = \frac{1}{3}\operatorname{tr} \mathbf{T}^3. \tag{6}$$

If the existence of a scalar function $W = W(\mathbf{T})$ is assumed such that $\boldsymbol{\varepsilon} = \mathfrak{f}(\mathbf{T}) = \frac{\partial W}{\partial \mathbf{T}}$, where W is an isotropic function, we obtain

$$\boldsymbol{\varepsilon} = W_1 \mathbf{I} + W_2 \mathbf{T} + W_3 \mathbf{T}^2. \tag{7}$$

In (7), $W_i = \frac{\partial W}{\partial I_i}$, where $i = 1, 2, 3$ and I_i has been defined previously.

[3] In the present communication, it is assumed that $|\nabla_X \mathbf{u}| \sim O(\delta)$, $\delta \ll 1$, which implies that only small strains and displacements are considered; therefore, it is not necessary to make an explicit distinction between the gradient operator with respect to the reference configuration ∇_X and the gradient operator with respect to the current configuration ∇.

Table 1 Values for the constants used in (8) and (9)

α	β (1/Pa)	γ (1/Pa)	ι (1/Pa^2)	E (Pa)	ν
0.01	9.277×10^{-8}	4.020×10^{-9}	10^{-14}	3.234×10^{8}	0.3

Equation (6) can be very useful to model the behaviour of elastic bodies, where stress concentration may appear but strains are always small. Let us consider in particular the expression:

$$W(I_1, I_2) = -\frac{\alpha}{\beta}\ln[\cosh(\beta I_1)] + \frac{\gamma}{\iota}\sqrt{1+2\iota I_2}, \quad \Rightarrow \quad \boldsymbol{\varepsilon} = -\alpha\tanh(\beta I_1)\mathbf{I} + \frac{\gamma}{\sqrt{1+2\iota I_2}}\mathbf{T}, \tag{8}$$

where α, β, γ, ι are constants given in Table 1.

The results for the boundary value problems using (8) will be compared with those obtained using the linearized constitutive equation for an isotropic elastic body

$$\boldsymbol{\varepsilon} = -\frac{\nu}{E}I_1\mathbf{I} + \frac{(\nu+1)}{E}\mathbf{T}, \tag{9}$$

where E is the Young's modulus and ν is the Poisson's ratio. The values of E and ν are presented in Table 1 and are adjusted such that when $|\mathbf{T}| \to 0$, the behaviour of an elastic body that results from using (8) and (9) is coincident (see Figures 1 and 2 in [10]). As remarked in Section 2.3 of [10] (see also Section 2.2 of [25] for a similar expression of W), this particular form for W has not been obtained from real experimental data, because (5) and (7) have been proposed very recently in the literature.

The particular expression for W presented in (8) has been proposed in [10] (see, in particular, Figures 1, 2 Section 2.3 therein) to study the behaviour of bodies that present 'large' stresses, but where strains are always small. In Fig. 1, we show some plots, where on the left results are presented for the axial ε_z and radial ε_r components of the strain, for a cylinder deforming under the influence of the uniform stress tensor distribution $\mathbf{T} = \sigma\mathbf{e}_z \otimes \mathbf{e}_z$, comparing (8) (denoted NL) and (9) (denoted L). On the right, results are presented for the shear deformation of a block deforming under the influence of the uniform shear stress $\mathbf{T} = \tau(\mathbf{e}_1 \otimes \mathbf{e}_2 + \mathbf{e}_2 \otimes \mathbf{e}_1)$, also comparing the results considering (8) and (9) (denoted by NL and L, respectively).

In Fig. 2, results are presented for the axial component of the strain ε_z for the same cylinder described above, under an axial uniform stress σ, considering different sets of values for the different constants that appear in (8), where for each case the values of the other parameters remain constant and are given in Table 1. This plot can help us to understand better the influence of the different material parameters in that model.

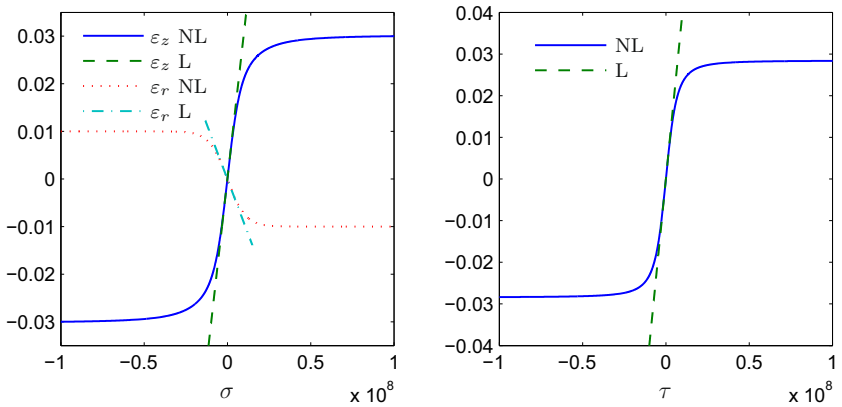

Fig. 1 On the *left*, behaviour of ε_z and ε_r for a cylinder under the influence of an axial uniform stress σ Pa. On the *right*, behaviour of the shear deformation for a block deforming due to the application of a uniform shear stress τ Pa

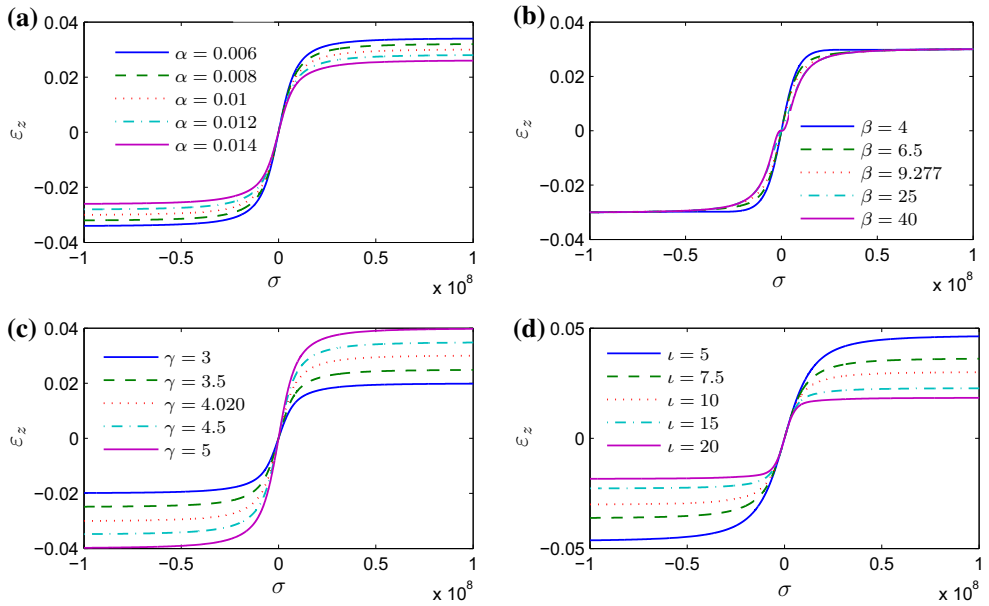

Fig. 2 ε_z as a function of σ Pa considering different possible values for constants in (8). **a** α, **b** $\beta \times 10^{-8}$ 1/Pa, **c** $\gamma \times 10^{-9}$ 1/Pa, **d** $\iota \times 10^{-15}$ 1/Pa^2

2.3 Boundary value problem

The boundary value problem consists in finding $\mathbf{T}$ and $\mathbf{u}$ from Eqs. (2), (7), and $(1)_3$, which for clarity of the exposition are written again as follows:

$$\operatorname{div} \mathbf{T} + \rho \mathbf{b} = \mathbf{0}, \tag{10}$$

$$\boldsymbol{\varepsilon} = W_1 \mathbf{I} + W_2 \mathbf{T} + W_3 \mathbf{T}^2, \tag{11}$$

$$\nabla \mathbf{u} + \nabla \mathbf{u}^{\mathrm{T}} = 2\boldsymbol{\varepsilon}, \tag{12}$$

with the boundary conditions

$$\mathbf{T}\mathbf{n} = \breve{\mathbf{t}} \quad \mathbf{x} \in \partial\kappa_r(\mathscr{B})_t, \quad \mathbf{u} = \breve{\mathbf{u}} \quad \mathbf{x} \in \partial\kappa_r(\mathscr{B})_u, \tag{13}$$

where $\breve{\mathbf{t}}$ is a given known external traction applied on the surface $\partial\kappa_r(\mathscr{B})_t$, $\mathbf{n}$ is the unit outward normal vector to $\partial\kappa_r(\mathscr{B})_t$, $\breve{\mathbf{u}}$ is a known displacement field on $\partial\kappa_r(\mathscr{B})_u$, and $\partial\kappa_r(\mathscr{B})$ is the boundary of the body $\kappa_r(\mathscr{B})_t$. In addition, it is assumed that $\partial\kappa_r(\mathscr{B})_t \cup \partial\kappa_r(\mathscr{B})_u = \partial\kappa_r(\mathscr{B})$ and $\partial\kappa_r(\mathscr{B})_t \cap \partial\kappa_r(\mathscr{B})_u = \emptyset$.

3 Numerical examples

In Sects. 3.1, 3.2, and 3.3, the boundary value problem (10)–(13) is solved using the finite element implementation presented in[4] Section 3 of [25], and we use the expression for W shown in (8) and we assume $\mathbf{b} = \mathbf{0}$. Three problems are analysed: the traction of a thin flat plate with hyperbolic boundaries, a semi-infinite medium (plane stress case) with a concentrated load applied on it, and a thin flat plate with an elliptic hole under traction applied sufficiently far from the hole. The numerical results obtained using (7) can be compared with the results considering (9), using well-known exact solutions that can be found, for example, in [14,18,35].

[4] It is necessary to mention that there is a typo in Eq. (20) of [25] where $\frac{\partial T_{ij}}{\partial \varepsilon_{kl}}$ is presented. The correct expression there should be

$$\frac{\partial T_{ij}}{\partial \varepsilon_{kl}} = -\frac{\alpha\beta}{(1+\beta I_1)^2}\delta_{ij}\delta_{kl} - \frac{\alpha\gamma\iota}{(1+2\iota I_2)^{3/2}} T_{ij}T_{kl} + \frac{\alpha\gamma}{\sqrt{1+2\iota I_2}}(\delta_{ik}\delta_{jl} + \delta_{jk}\delta_{il}),$$

where the constants α, β, γ, and ι belong to a different model for W as the one used in the present communication.

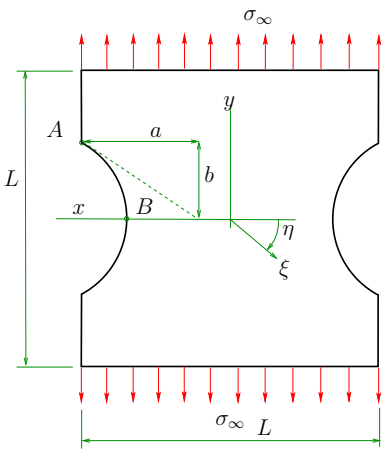

Fig. 3 Sketch of a plane plate with hyperbolic boundaries under traction

Table 2 Values for the dimensions of the plate with hyperbolic boundaries

$L = 1\,\text{m}$	$b = 0.1\,\text{m}$	$\frac{a}{b}$:	1/10	1/5	1/2	1	2	3

3.1 Plane plate with hyperbolic boundaries

A sketch of a flat plate with hyperbolic boundaries is presented in Fig. 3. This plate is under the action of a uniform load σ_∞ acting sufficiently far from the hyperbolic boundaries. The dashed line represents the tangent line to the hyperbolic boundary at point A. It is assumed that L is sufficiently large (in comparison with a and b) such that the stresses and strains are uniform sufficiently far from the hyperbolic boundaries and the thickness of the plate is very small in comparison with a and b. As a result, this problem is solved assuming a plane stress condition. In the present work, L and b are fixed and different values are considered for a as presented in Table 2.

For a very large plate with hyperbolic boundaries and using (9), the boundary value problem (10)–(13) has the exact solution[5] (see Fig. 3)

$$T_{\xi\xi} + T_{\eta\eta} = 4\Re[\psi'(z)], \tag{14}$$

$$T_{\eta\eta} - T_{\xi\xi} + 2iT_{\xi\eta} = 2e^{2i\alpha}[\bar{z}\psi''(z) + \chi''(z)], \tag{15}$$

where

$$\psi(z) = -\frac{Ai\zeta}{2}, \quad \chi(z) = -\frac{Ai\zeta}{2} - Bci\sinh(\zeta), \tag{16}$$

and

$$\zeta = \xi + i\eta, \quad A = -\frac{\sigma_\infty L}{\pi - 2\eta_0 + \sin(2\eta_0)}, \quad B = -A\cos^2(\eta_0), \tag{17}$$

where L is the width of the plate (see Fig. 3), α is the angle between the tangent line defined by $\eta =$ constant and the axis x, and

$$c = \sqrt{a^2 + b^2}, \quad \eta_0 = \arctan(b/a). \tag{18}$$

When $\eta = 0$, the co-ordinate ξ coincides with x and $T_{\xi\xi} = T_{11}$, $T_{\eta\eta} = T_{22}$, and $T_{\xi\eta} = T_{12}$.

Because of symmetry, only a quarter of the plate is considered for the finite element model. Linear quadrilateral elements have been used for this and for the rest of the examples presented in this paper.

[5] See, for example, [14] and also the original works by Griffith [15] and Neuber [23].

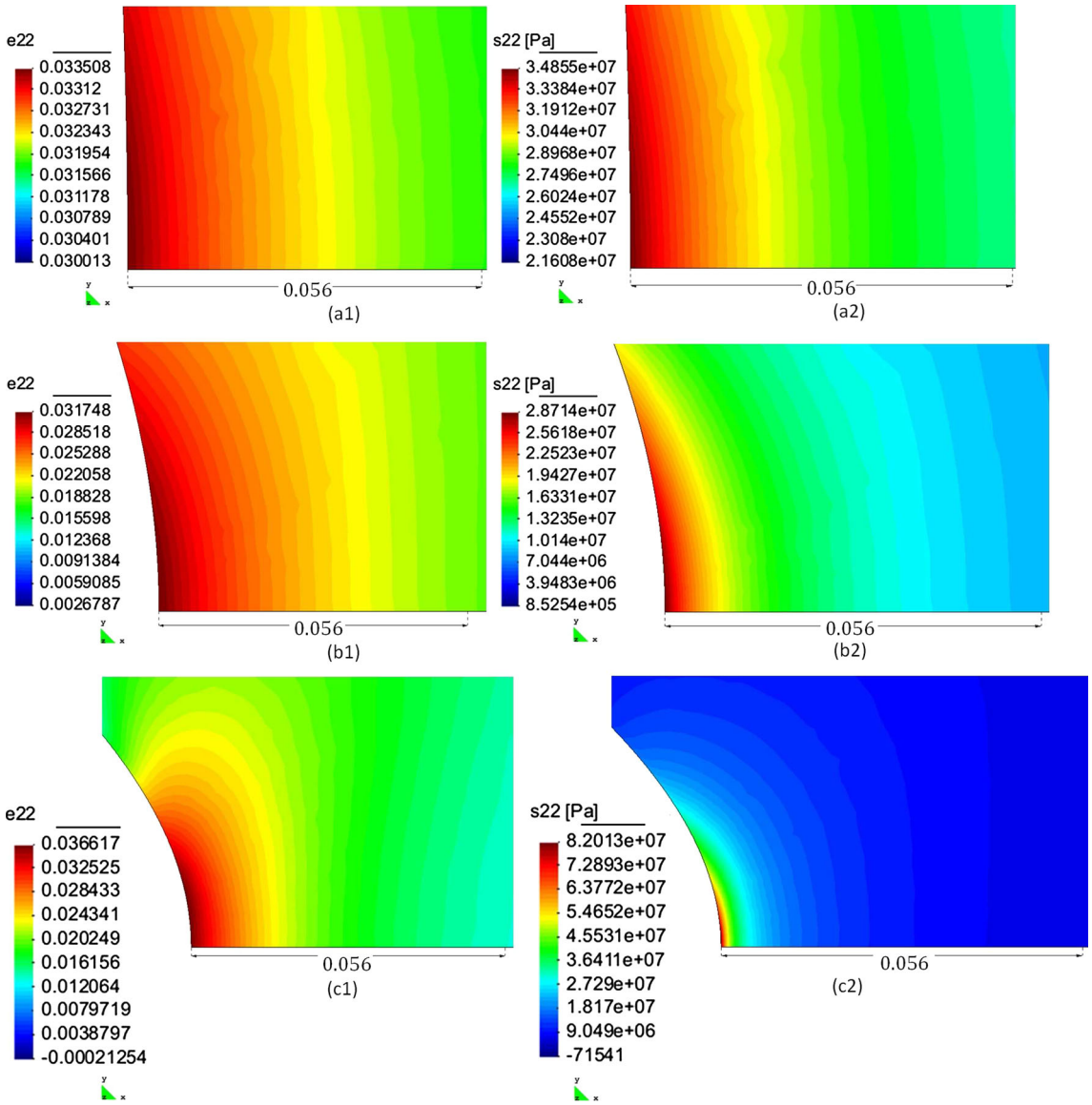

Fig. 4 **a1** and **a2** are the *contour plots* for ε_{22} and T_{22} (in Pa), respectively, with $\sigma_\infty = 2.5 \times 10^7$ Pa and $\frac{a}{b} = \frac{1}{10}$; **b1** and **b2** are the *contour plots* for ε_{22} and T_{22} (in Pa), respectively, with $\sigma_\infty = 5 \times 10^6$ Pa and $\frac{a}{b} = 1$; **c1** and **c2** are the *contour plots* for ε_{22} and T_{22} (in Pa), respectively, with $\sigma_\infty = 2.6 \times 10^6$ Pa and $\frac{a}{b} = 3$

In Figure 6.30 of [22], results are presented[6] for $\bar{T}_{22} = \frac{T_{22}}{\sigma_\infty}$ and ε_{22} in terms of the natural logarithm of the degrees of freedom DOF where for a refined mesh, the results would be independent of the element size. More details regarding the mesh used for the different cases presented in Table 2 can be also be found in pp.79–86 of [22]. For brevity, such results are not presented here.

As mentioned in the Introduction, one of the possible uses of (7) is in problems involving concentrations of stresses for brittle bodies, where we can expect that 'large' stresses can be obtained, while strains remain small. In Fig. 4, results are presented for the fields ε_{22} and T_{22} near point[7] B (see Fig. 3) and for $\frac{a}{b} = \frac{1}{10}$, $\frac{a}{b} = 1$, and $\frac{a}{b} = 3$, respectively. It is observed that when $\frac{a}{b} = 3$, which represents the case where the concentration of stresses near B is higher, the strains remain small and the distribution is less concentrated around B.

[6] The results are presented for point B (see Fig. 3) and for $\frac{a}{b} = 3$.

[7] In the contour plots presented here and in the next sections, the components ε_{22}, T_{22}, ε_{11}, and T_{11} are denoted by $e22$, $s22$, $e11$, and $s11$, respectively.

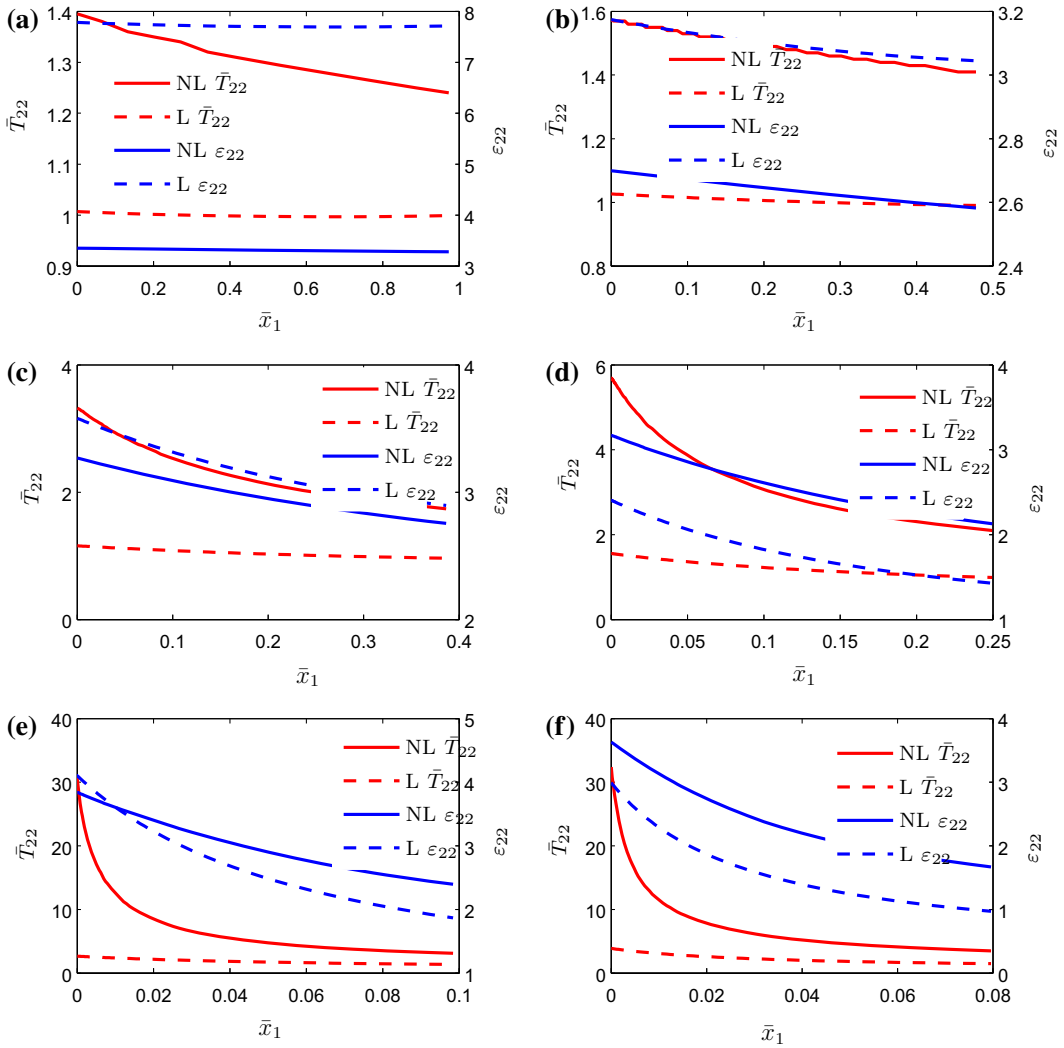

Fig. 5 Plate with hyperbolic boundaries. Results for $\bar{T}_{22}$ (see scales on the *left*) and ε_{22} (in %, see scales on the *right*) for different relations for $\frac{a}{b}$, with the material described by the nonlinear constitutive relation (8) (denoted by NL), and the results obtained from the linearized theory (9) (denoted by L). **a** $\frac{a}{b} = \frac{1}{10}$ with $\sigma_\infty = 2 \times 10^7$ Pa; **b** $\frac{a}{b} = \frac{1}{5}$ with $\sigma_\infty = 10^7$ Pa; **c** $\frac{a}{b} = \frac{1}{2}$ with $\sigma_\infty = 10^7$ Pa; **d** $\frac{a}{b} = 1$ with $\sigma_\infty = 5 \times 10^6$ Pa; **e** $\frac{a}{b} = 2$ with $\sigma_\infty = 5 \times 10^6$ Pa; **f** $\frac{a}{b} = 3$ with $\sigma_\infty = 2.5 \times 10^6$ Pa

For the results presented in Fig. 5, the origin of the coordinate system has been translated to point B. In those plots, results for ε_{22} and T_{22} are presented, for the full spectrum of the ratio $\frac{a}{b}$ given in Table 2, and compared with the results that are predicted by the linearized theory of elasticity (14)–(18).

In these plots,

$$\bar{x} = \frac{x - x_a}{x_a}, \quad x_a = a\left[\cosh\left(\frac{\pi}{2}\right) - 1\right]. \tag{19}$$

Finally, in Fig. 6 results are presented for ε_{22} and T_{22} for $\frac{a}{b} = 3$ with different external traction σ_∞.

3.2 Concentrated force at a point on a straight boundary

In this section, some results are presented for the classical problem of a semi-infinite medium deforming due to the application of a point load, as depicted in Fig. 7. The body is assumed to be very thin in the direction z, so the plane stress formulation is appropriate for this setting.

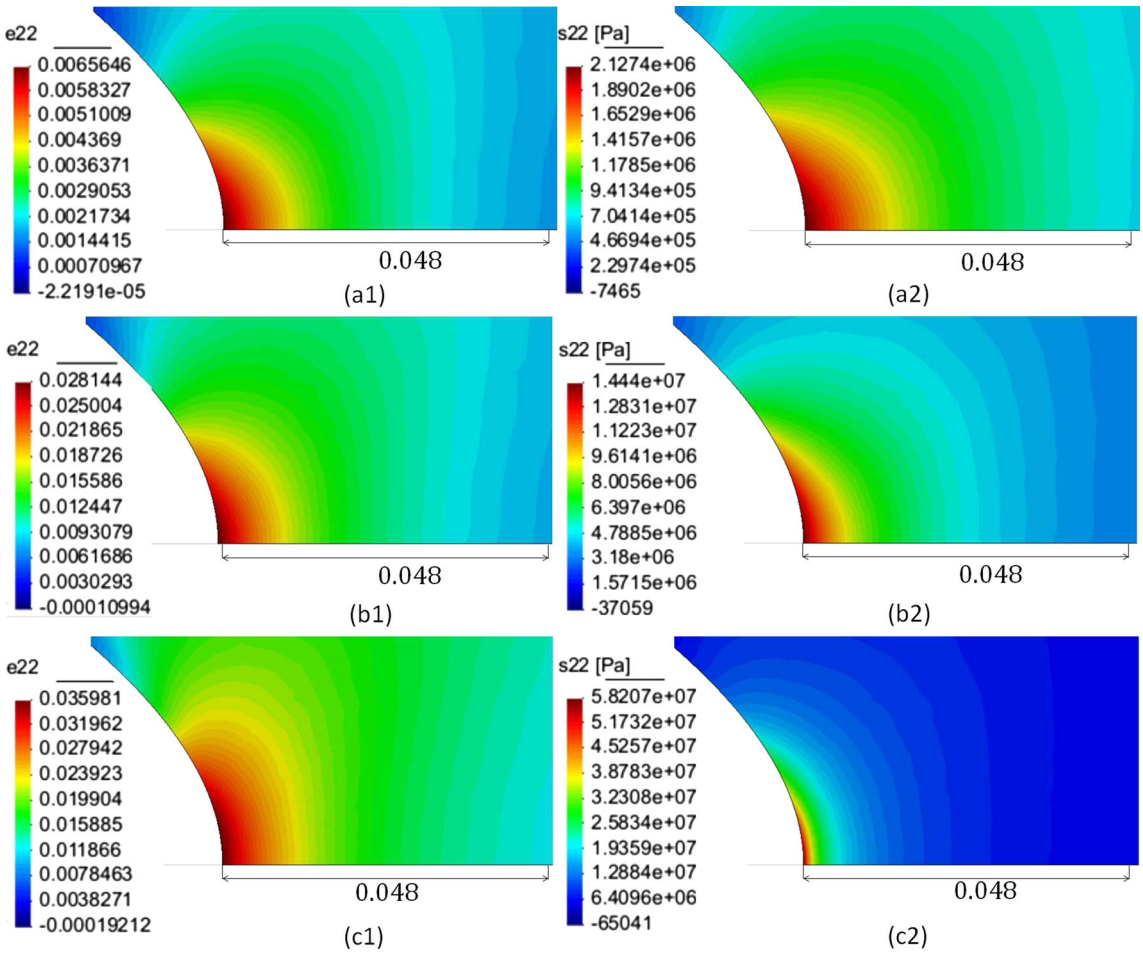

Fig. 6 **a1** and **a2** are the *contour plots* for ε_{22} and T_{22} (in Pa), respectively, with $\sigma_\infty = 250{,}000$ Pa; **b1** and **b2** are the *contour plots* for ε_{22} and T_{22} (in Pa), respectively, with $\sigma_\infty = 1{,}250{,}000$ Pa; **c1** and **c2** are the *contour plots* for ε_{22} and T_{22} (in Pa), respectively, with $\sigma_\infty = 2{,}250{,}000$ Pa

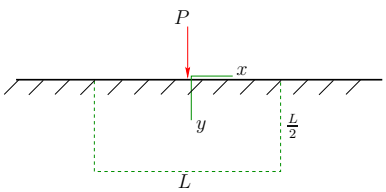

Fig. 7 Semi-infinite medium with a point load applied on it

When the classical relation (9) is used and a force $\mathbf{P} = P_1\mathbf{e}_1 + P_2\mathbf{e}_2$ is applied on the semi-infinite medium, this problem has the exact solution (see, for example, [18] and the original works by Boussinesq [1] and Flamant [12]):

$$T_{11} = -\frac{P_1(1+\nu)}{4\pi}\frac{x}{(x^2+y^2)}\left[\frac{2}{1+\nu}+\frac{(x^2-y^2)}{(x^2+y^2)}\right] - \frac{P_2(1+\nu)}{4\pi}\frac{y}{(x^2+y^2)}\left[\frac{2\nu}{1+\nu}+\frac{(x^2-y^2)}{(x^2+y^2)}\right], \quad (20)$$

$$T_{22} = -\frac{P_1(1+\nu)}{4\pi}\frac{x}{(x^2+y^2)}\left[\frac{2}{1+\nu}-\frac{(x^2-y^2)}{(x^2+y^2)}\right] - \frac{P_2(1+\nu)}{4\pi}\frac{y}{(x^2+y^2)}\left[\frac{2}{1+\nu}-\frac{(x^2-y^2)}{(x^2+y^2)}\right], \quad (21)$$

$$T_{12} = -\frac{P_1(1+\nu)}{4\pi}\frac{x}{(x^2+y^2)}\left[\frac{1-\nu}{1+\nu}+\frac{2x^2}{(x^2+y^2)}\right] - \frac{P_2(1+\nu)}{4\pi}\frac{x}{(x^2+y^2)}\left[\frac{1-\nu}{1+\nu}-\frac{2y^2}{(x^2+y^2)}\right], \quad (22)$$

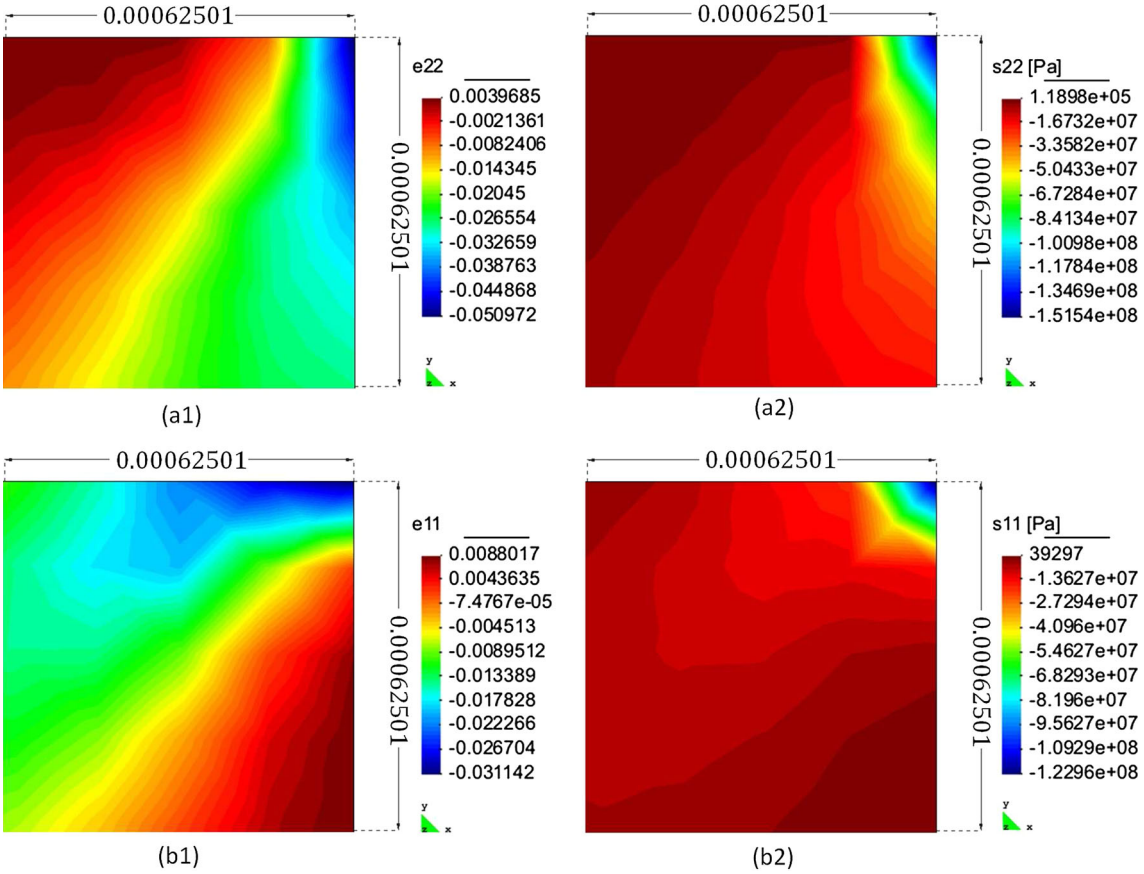

Fig. 8 a1, **a2**, **b1**, and **b2** are the *contour plots* for ε_{22}, T_{22}, ε_{11}, and T_{11} (components of the stress in Pa), respectively, with $P = 10^4$ N

which predicts stresses whose magnitudes go to infinite as one approaches the point where the load is applied; however, from (9), such a solution would also predict strains whose magnitudes would go to infinite near the point of application of the load, which contradicts the basic assumption of the linearized theory of elasticity (see [31] and the introduction section in [3]).

In this section, we show that using (7) with the expression for W proposed in (8), stresses can be very 'large' but strains remain small.

Equations (10)–(13) are solved using (8) and the finite element method. To deal with the semi-infinite setting, we use a finite size plate of sides L, $\frac{L}{2}$, as depicted as dashed lines in Fig. 7. The hypothesis is that for L 'large' enough, the results for ε_{ij} and T_{ij} near the point of application of P are not significantly affected by such value of L. That is indeed the case as presented in Figures 6.42 of [22], which for brevity are not shown here. For the results presented in this work, we have assumed that $L = 4$ m. Because of the symmetry of the problem (see the location of the co-ordinates $x - y$), only one half of the plate is considered for the numerical analysis.

In Figure 6.49 of [22], results are presented for ε_{22} and $\bar{T}_{22} = \frac{T_{22}}{\sigma_\infty}$ as functions of the natural logarithm of the degrees of freedom DOF, where ε_{22} and $\bar{T}_{22}$ have been evaluated at point $(x, y) = (0, y)$ with y very close[8] to 0. For brevity, again such results are not presented in this communication.

In this problem, only one geometry is necessary for the numerical analysis. In Fig. 8, results for $\varepsilon_{11}, \varepsilon_{22}, T_{11}$, and T_{22} near the point of application of $P = 10^4$ N are presented. It is interesting to observe the differences in the distributions for the normal components of the stress tensor, when compared with the way the longitudinal

[8] From the point of view of the numerical results, it is not possible to evaluate T_{22} exactly at $(x, y) = (0, 0)$, because in that point T_{22} is expected to go to infinite.
The stress σ_∞ is calculated in the following way. Consider (20)–(22) with $P_1 = 0$, $P_2 = P$ and evaluate T_{22} at point $(x, y) = (0, L)$ to obtain $\sigma_\infty = -\frac{P(3+\nu)}{4\pi L}$, which is the value used to obtain the dimensionless expression $\bar{T}_{22}$ above.

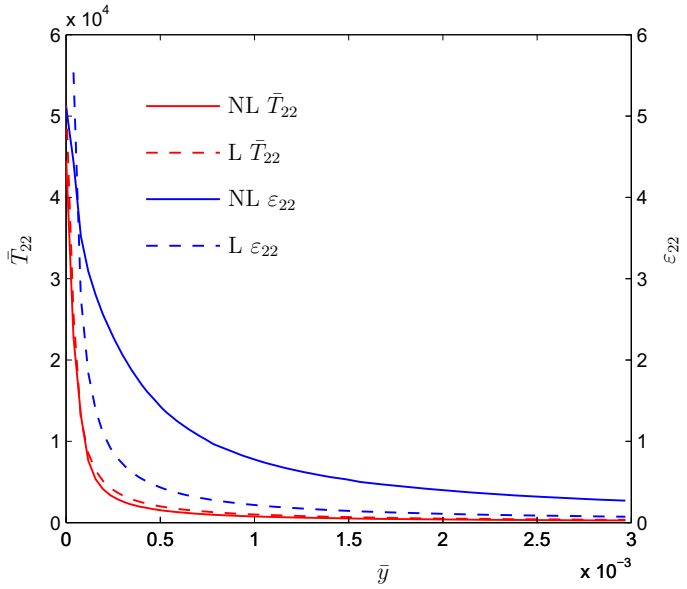

Fig. 9 Half-space with a point load applied on it. Results for $\bar{T}_{22}$ (see scale on the *left*) and ε_{22} (in %, see scale on the *right*) for the *line* $(0, y)$ with the material described by nonlinear constitutive relation (8) (denoted by NL) and the linearized theory (9) (denoted by L, see (20)–(22). The external load is $P = 10^4$ N

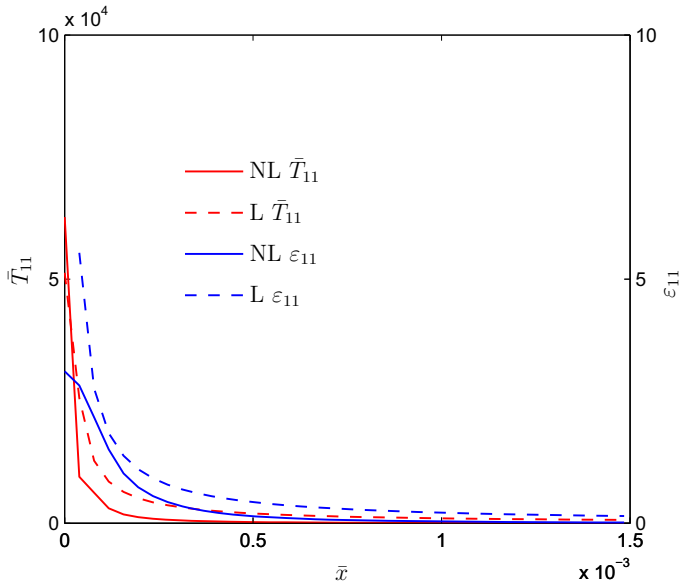

Fig. 10 Half-space with a point load applied on it. Results for $\bar{T}_{11}$ (see scale on the *left*) and ε_{11} (in %, see scale on the *right*) for the line $(x, 0)$ with the material described by the nonlinear constitutive relation (8) (denoted by NL) and the linearized theory (9) (denoted by L, see (20)–(22). The external load is $P = 10^4$ N

components of the linearized strain tensor behave. In Fig. 8, a zooming into the tip is shown to better observe the 'size' of the zone of stresses and strains concentrations. We also observe that strains remain small.

Figures 9 and 10 present results for ε_{11}, $\bar{T}_{11} = \frac{T_{11}}{\sigma_\infty}$ as functions of $\bar{x} = \frac{x}{L}$, and ε_{22}, $\bar{T}_{22}$ as functions of $\bar{y} = \frac{y}{L}$, respectively, using the new constitutive theory (7), (8), and the constitutive equation for the linearized theory of elasticity (9) (see (20)–(22). In Fig. 9, results are shown for the line $(0, y)$, whereas the results presented in Fig. 10 are obtained for the line $(x, 0)$.

In Fig. 11, results for ε_{22} and T_{22} (contour plots) are presented for different external loads P.

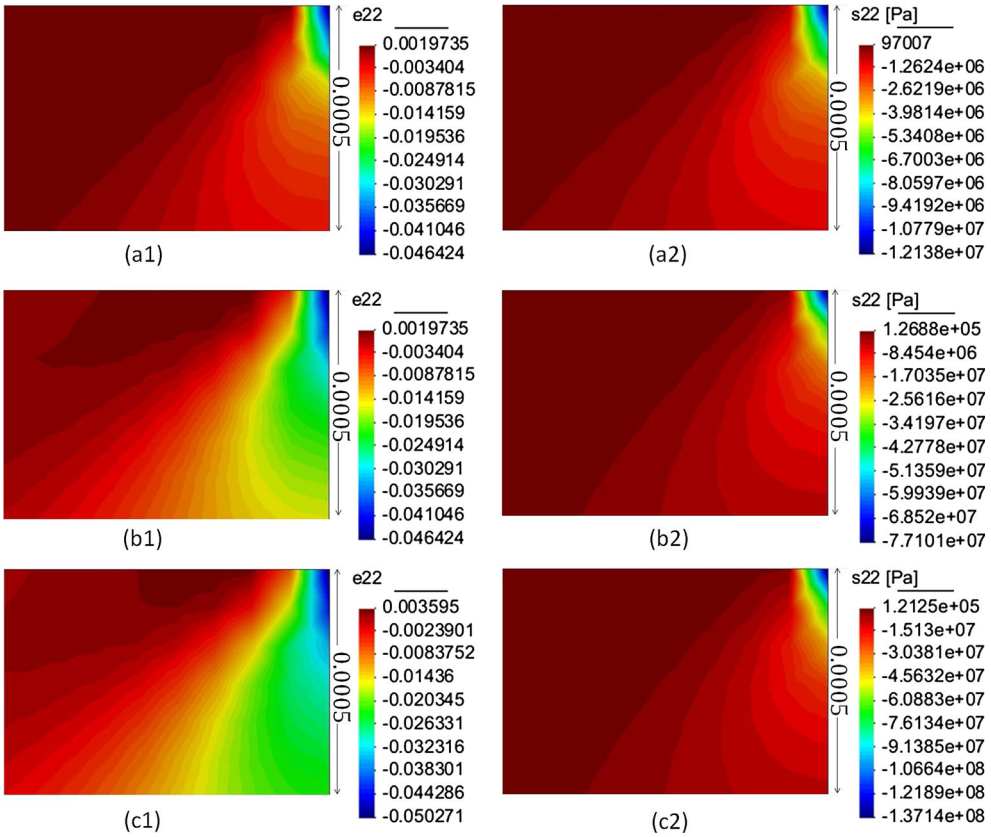

Fig. 11 **a1** and **a2** are the *contour plots* for ε_{22} and T_{22} (in Pa), respectively, with $P = 1000$ N; **b1** and **b2** are the *contour plots* for ε_{22} and T_{22} (in Pa), respectively, with $P = 5000$ N; **c1** and **c2** are the *contour plots* for ε_{22} and T_{22} (in Pa), respectively, with $P = 9000$ N

3.3 Elliptic hole in an uniformly stressed plate

In this section, results are presented for the problem of a thin plate under uniform traction σ_∞ applied sufficiently far from a central elliptic hole. The results shown here complement the solutions already published in [25] for the same problem. Here, additional relations between the semi-axes of the elliptic hole are considered. In Fig. 12, a schematic depiction of the plate is presented. The semi-axes of the elliptic hole are denoted by a and

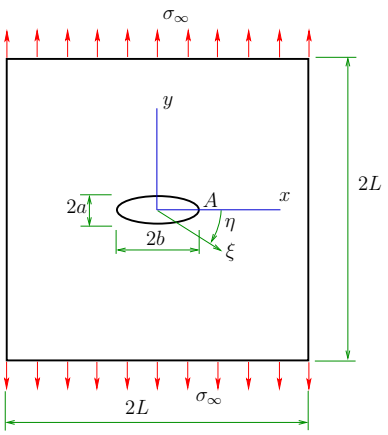

Fig. 12 A thin flat plate with an elliptic hole under traction. Point A is located at $(x, y) = (b, 0)$

Table 3 Values for the semi-axes of the elliptic hole

$\frac{a}{b}$	1/25	1/30	1/35	1/40	1/45	1/50

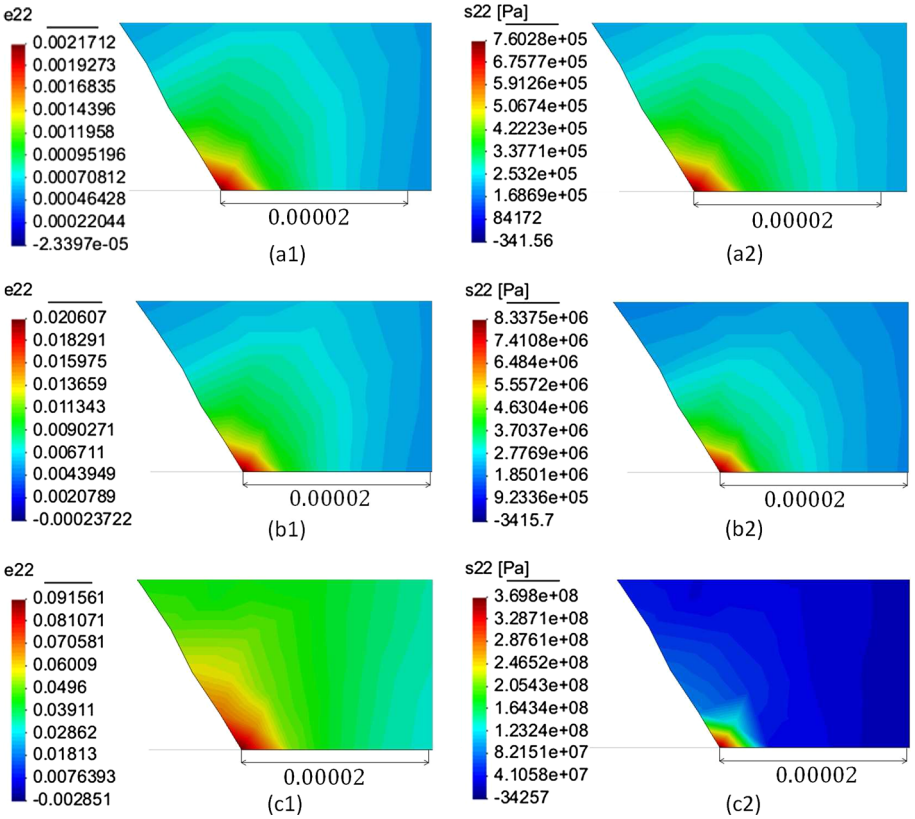

Fig. 13 **a1** and **a2** are the *contour plots* for ε_{22} and T_{22} (in Pa), respectively, with $\sigma_\infty = 5000$ Pa; **b1** and **b2** are the *contour plots* for ε_{22} and T_{22} (in Pa), respectively, with $\sigma_\infty = 50{,}000$ Pa; **c1** and **c2** are the *contour plots* for ε_{22} and T_{22} (in Pa), respectively, with $\sigma_\infty = 500{,}000$ Pa

b. The list of cases that are considered is presented in Table 3. These cases complement the results presented in [25], where the minimum value for $\frac{a}{b}$ was $\frac{1}{20}$.

When the linearized constitutive relation (9) is considered, the boundary value problem has the same exact solution presented in the previous section, where in this case[9]

$$4\psi(z) = \sigma_\infty c\left[e^{2\xi_0}\cosh\zeta + \left(1 - e^{2\xi_0 - 2i\beta}\right)\sinh\xi\right], \tag{23}$$

$$4\chi(z) = -\sigma_\infty c^2\left[\left(\cosh(2\xi_0) - \cosh(2\beta)\right)\zeta + \frac{1}{2}e^{2\xi_0}\cosh(2(\zeta - \xi_0 - i\beta))\right], \tag{24}$$

with $\beta = 0$ and z, c, ζ, and α already defined in Sect. 3.1. When $\eta = 0$, the axis ξ is equivalent to x and $T_{\xi\xi} = T_{11}$, $T_{\eta\eta} = T_{22}$, and $T_{\xi\eta} = T_{12}$.

In this work, it is assumed that $L = 1$ m and $b = 0.1$ m. On considering such dimensions, it is possible to show that the model is close to what can be considered as an 'infinite' plate; i.e. for L longer than 1 m, there are slightly negligible differences among the distributions of ε_{ij}, T_{ij}, and u_i (in terms of L) for a given σ_∞ (see [22]).

Because of the symmetries of the problem, only a quarter of the plate is considered. Due to the expected high concentration of stresses for $\frac{a}{b} = \frac{1}{50}$ (see Table 3), it is necessary to have refined meshes for the finite

[9] See, for example, [35] and the original works by Inglis [16] and Kolosoff [20].

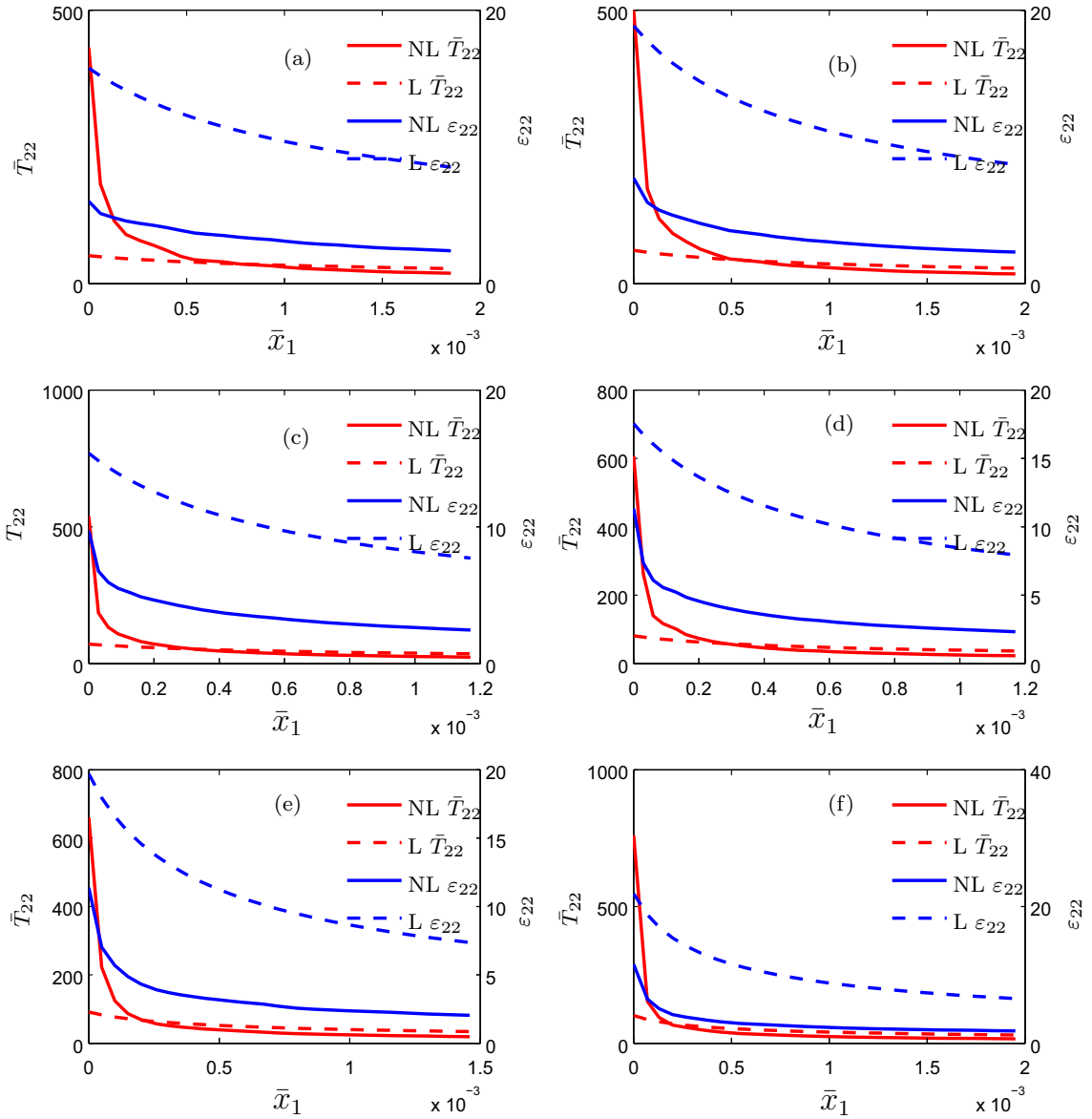

Fig. 14 Plate with an elliptic hole. Results for $\bar{T}_{22}$ (see scales on the *left*) and ε_{22} (in %, see scales on the *right*) for different relations for $\frac{a}{b}$ with the material defined by the nonlinear constitutive relation (8) (denoted by NL) and the linearized theory (9) (denoted by L). **a** $\frac{a}{b} = \frac{1}{25}$ with $\sigma_\infty = 10^6$ Pa; **b** $\frac{a}{b} = \frac{1}{30}$ with $\sigma_\infty = 10^6$ Pa; **c** $\frac{a}{b} = \frac{1}{35}$ with $\sigma_\infty = 7 \times 10^5$ Pa; **d** $\frac{a}{b} = \frac{1}{40}$ with $\sigma_\infty = 7 \times 10^5$ Pa; **e** $\frac{a}{b} = \frac{1}{45}$ with $\sigma_\infty = 7 \times 10^5$ Pa; **f** $\frac{a}{b} = \frac{1}{50}$ with $\sigma_\infty = 7 \times 10^5$ Pa

elements around point A (see Fig. 12). In Figure 6.10 of [22], results are presented for ε_{22} and T_{22} evaluated at point A in terms of the natural logarithm of the number of degrees of freedom DOF of the finite element model for the cases $\frac{a}{b} = \frac{1}{25}, \frac{1}{30}, \frac{1}{35}, \frac{1}{40}$, and $\frac{1}{50}$. From that figure, it is seen that the results become approximately constant for larger number of DOF; however, the same is not apparent for the cases $\frac{a}{b} = \frac{1}{45}$ and $\frac{a}{b} = \frac{1}{50}$; therefore, for the results shown below, care must be taken when considering those cases. As in the previous two sections, for brevity such results are not presented here.

In Fig. 13, results are presented for ε_{22} and T_{22} for different magnitudes of σ_∞ near the point A. To compare the size of the zone where the concentration of the stresses and strains happens, special attention must be paid to the scale presented in each figure. Note that in these three cases (see pp. 65–67 and Figure 6.12 of [22] for similar results), the strains remain small and the distributions for ε_{22} are 'smoother' than for T_{22}.

Figure 14 presents the results for ε_{22} and $\bar{T}_{22} = \frac{T_{22}}{\sigma_\infty}$, for the line $(x, y) = (x, 0)$, starting from point A to the right, where $\bar{x} = \frac{x-b}{b}$, and using the cases listed in Table 3. These results are juxtaposed with the results that are obtained from the constitutive models (8) and (9).

4 Conclusions

In this work, we have presented some numerical solutions for some boundary value problems, considering a relatively new class of constitutive relation, where the linearized strain tensor is assumed to be a nonlinear function of the Cauchy stress, in the particular case where we can observe strain-limiting behaviour (see Fig. 1). The hypothesis is that such models could be used to study the behaviour of brittle bodies when there is stress concentration. Three boundary value problems have been considered, where we observe stress concentration but where we can see that strains remain small, unlike the case of using the linearized constitutive relation (9), where strains can also be large (see, for example, Figs. 10 and 14), which is a contradiction with one of the main assumptions of the linearized theory of elasticity.

In future works, actual experimental data will be used to propose more realistic expressions for the functions in (5), and more boundary value problems will be solved, in particular considering time effects.

Acknowledgments The authors would like to express his gratitude for the financial support provided by FONDECYT (Chile) under Grant No. 1120011. The work of S. Montero was also funded by a Scholarship for master degree students provided by CONICYT (Chile).

References

1. Boussinesq, J.: Applications des potentials à l'étude de l'équilibre et du mouvement des solids élastique. Gauthier-Villars, Paris (1885)
2. Bridges, C., Rajagopal, K.R.: Implicit constitutive models with a thermodynamic basis: a study of stress concentration. Z. Angew. Math. Phys. **66**, 191–208 (2015)
3. Bulíček, M., Málek, J.: On elastic solids with limiting small strain: modelling and analysis. EMS Surv. Math. Sci. **1**, 283–332 (2014)
4. Bulíček, M., Málek, J., Rajagopal, K.R., Walton, J.R.: Existence of solutions for the anti-plane stress for a new class of 'strain-limiting' elastic bodies. Calc. Var. (2015). doi:10.1007/s00526-015-0859-5
5. Bustamante, R.: Some topics on a new class of elastic bodies. Proc. R. Soc. A **465**, 1377–1392 (2009)
6. Bustamante, R., Rajagopal, K.R.: A note on plain strain and stress problems for a new class of elastic bodies. Math. Mech. Solids **15**, 229–238 (2010)
7. Bustamante, R., Rajagopal, K.R.: Solutions of some simple boundary value problems within the context of a new class of elastic materials. Int. J. Nonlinear Mech. **46**, 376–386 (2011)
8. Bustamante, R., Rajagopal, K.R.: On the inhomogeneous shearing of a new class of elastic bodies. Math. Mech. Solids **17**, 762–778 (2011)
9. Bustamante, R., Sfyris, D.: Direct determination of stresses from the stress wave equations of motion and wave propagation for a new class of elastic bodies. Math. Mech. Solids **20**, 80–91 (2015)
10. Bustamante, R., Rajagopal, K.R.: Solutions of some boundary value problems for a new class of elastic bodies undergoing small strains. Comparison with the predictions of the classical theory of linearized elasticity: part I. Problems with cylindrical symmetry. Acta Mech. **226**, 1815–1838 (2015)
11. Chadwick, P.: Continuum Mechanics: Consice Theory and Problems. Dover Publications INC, Mineola New York (1999)
12. Flamant, M.: Sur la rèpartition des pressions dans un solide rectangulaire chargé transversalement. Compt. Rend. **114**, 1465–1468 (1892)
13. Gou, K., Muddamallappa, M., Rajagopal, K.R., Walton, J.R.: Modeling fracture in the context of a strain limiting theory in elasticity: a single plane-strain crack. Int. J. Eng. Sci. **88**, 73–82 (2015)
14. Green, A.E., Zerna, W.: Theoretical Elasticity, 2nd edn. Dover Publications Inc., New York (1968)
15. Griffith, A.A.: Stresses in a plate bounded by a hyperbolic cylinder. Tech. Rep. Aeronaut. Res. Commun. **II**, 668–677 (1927–1928)
16. Inglis, C.E.: Stresses in a plate due to the presence of cracks and sharp corners. Trans. Inst. Nav. Archit. **55**, 219–230 (1913)
17. Johnson, P.A., Rasolfosaon, P.N.J.: Manifestation of nonlinear elasticity in rock: convincing evidence over large frequency and strain intervals from laboratory studies. Nonlinear Process. Geophys. **3**, 77–88 (1996)
18. Kachanov, M., Sharifo, B., Tsukrov, I.: Handbook of Elasticity Solutions, 13th edn. Springer Science, Berlin (2003)
19. Kannan, K., Rajagopal, K.R., Saccomandi, G.: Unsteady motions of a new class of elastic solids. Wave Motion **51**, 833–843 (2014)
20. Kolosoff, G.: On some properties of problems in the plane theory of elasticity. Z. Math. Physik **62**, 384–409 (1914)
21. Kulvait, V., Malek, J., Rajagopal, K.R.: Anti-plane stress state of a plate with a V-notch for a new class of elastic solids. Int. J. Fract. **179**, 59–73 (2013)

22. Montero, S.: Solución numérica de algunos problemas de valor de frontera para un nuevo tipo de ecuación constitutiva considerando pequeñas deformaciones y comportamiento no lineal de sólido. Master's Thesis, Departamento de Ingeniería Mecánica, Universidad de Chile (2014)
23. Neuber, H.: Elastich-strenge lösungen zur kerbwirkung bei scheiben und umdrehungskörpen. Z. Angew. Math. Mech. **13**, 439–442 (1933)
24. Ortiz, A., Bustamante, R., Rajagopal, K.R.: A numerical study of a plate with a hole for a new class of elastic bodies. Acta Mech. **223**, 1971–1981 (2012)
25. Ortiz-Bernardin, A., Bustamante, R., Rajagopal, K.R.: A numerical study of elastic bodies that are described by constitutive equations that exhibit limited strains. Int. J. Solids Struct. **51**, 875–885 (2014)
26. Rajagopal, K.R.: On implicit constitutive theories. Appl. Math. **48**, 279–319 (2003)
27. Rajagopal, K.R.: The elasticity of elasticity. Z. Angew. Math. Phys. **58**, 309–317 (2007)
28. Rajagopal, K.R., Srinivasa, A.R.: On the response of non-dissipative solids. Proc. R. Soc. A **463**, 357–367 (2007)
29. Rajagopal, K.R., Srinivasa, A.R.: On a class of non-dissipative solids that are not hyperelastic. Proc. R. Soc. A **465**, 493–500 (2009)
30. Rajagopal, K.R.: Conspectus of concepts of elasticity. Math. Mech. Solids **16**, 536–562 (2011)
31. Rajagopal, K.R.: On the nonlinear elastic response of bodies in the small strain range. Acta Mech. **225**, 1545–1553 (2014)
32. Saito, T., Furuta, T., Hwang, J.H., Kuramoto, S., Nishino, K., Susuki, N., Chen, R., Yamada, A., Ito, K., Seno, Y., Nonaka, T., Ikehata, H., Nagasako, N., Iwamoto, C., Ikuhara, Y., Sakuma, T.: Multifunctional alloys obtained via a dislocation-free plastic deformation mechanism. Science **300**, 464–467 (2003)
33. Spencer, A. J. M.: Theory of invariants. In: Eringen, A.C. (ed.) Continuum Physics, vol. 1., pp. 239–353. Academic Press, New York (1971)
34. Talling, R.J., Dashwood, R.J., Jackson, M., Kuramoto, S., Dye, D.: Determination of $C_{11} - C_{12}$ in Ti–36Nb–2Ta–3Zr–0.3O (xt.%) (gum metal). Scripta Mater. **59**, 669–672 (2008)
35. Timoshenko, S.P., Goodier, J.N.: Theory of Elasticity, 2nd edn. McGraw Hill Inc., New York (1970)
36. Truesdell, C.A., Toupin, R.: The classical field theories. In: Handbuch der Physik, Vol.III/1. Berlin: Springer (1960)